Supplement to Stopsack *et al*., **Multiplex immunofluorescence in formalin-fixed paraffin-embedded tumor tissue to identify single cell-level PI3K pathway activation**

Supplementary Methods: Machine learning

Two additional data-driven machine learning approaches were used to quantify cell-level PI3K activation based on cell-level PTEN, pS6, and stathmin intensity values. Values were first quantile normalized and square root transformed to improve normality. In the first approach, principal components analysis was performed.

In the second approach, unsupervised clustering on a cell level with Clustering Large Applications (CLARA) (45) was used, a big-data implementation of the partitioning around medoids (PAM) algorithm. Three to five clusters were chosen, as suggested by the gap statistic and silhouette and elbow methods. Each tumor was assigned the cluster most common among its cells. The degree of admixture within each tumor was measured as the proportion of tumor cells within each tumor that did not correspond to the most common cluster of that tumor (mode). For visualization of clusters, the Barnes-Hut implementation of *t*-distributed stochastic neighbor embedding (t-SNE) was used (46).

Supplementary Text: Results

mRNA signatures in TCGA

Without a signature of PI3K activation specific to primary prostate cancer at hand that had been validated in clinical prostate cancer samples, we tested a widely used transcriptomic signature of PTEN loss derived in breast cancer (30) but found it not to be associated with PTEN status in HPFS and PHS and only modestly different by *PTEN* copy number status in prostate tumors from TCGA (Fig. S2.A–B).

To fill this gap, we derived a novel prostate cancer-specific signature in TCGA (Fig. S2.C; Table S2). The signature predominantly reflects transcriptional effects of *PTEN* loss, as 95 of the 333 patients in TCGA (29%) had *PTEN* alterations (93 of them deletions) and only 8 patients (2%) had *PIK3CA* or *PIK3CB* mutations.

Validating our transcriptome signature among tumors from the HPFS and PHS cohorts with both tumor-level PTEN status and transcriptome profiling (n = 226), the overall accuracy of discrimination between PTEN-intact tumors and tumors with PTEN loss was high (area under the curve, 0.79; 95% CI, 0.71 to 0.86), considerably higher than the above-mentioned signature previously derived in breast cancer (30) (area under the curve, 0.54; 95% CI, 0.44 to 0.64). Tumors with complete PTEN loss had a higher PI3K transcriptome signature score than PTEN-intact tumors (Fig. S2.D). While tumors with heterozygous *PTEN* deletions in TCGA had markedly higher scores for the mRNA signature (Fig. S2.C), we did not observe clear differences in scores for tumors with heterogeneous PTEN loss compared to tumors scored as PTEN-intact (difference, 10 points; 95% CI, –9 to 29; Fig. S2.D). These observations underscore that spatially heterogeneous PTEN protein expression is a distinct phenomenon from single-allele *PTEN* copy number alterations on bulk tumor DNA sequencing.

We additionally compiled a PI3K activation gene list derived in cell lines (not human samples) treated with older PI3K inhibitors, into a signature (29). This signature was associated with *PTEN* copy number status in TCGA, with PTEN immunohistochemistry in HPFS/PHS, and with our PI3K scores.

To test the validity of the individual markers, we compared PTEN, pS6, and stathmin levels individually with tumor-level PTEN status and the transcriptome signatures (Fig. S2.H–J).

Intratumoral heterogeneity

In most tumors, cells with higher PTEN expressions had lower pS6 expression, but not in all tumors (median r within a tumor, –0.18; IQR across tumors, –0.41 to 0.06). Higher cell-level PTEN levels were generally correlated with higher stathmin levels within a tumor (median r, 0.26; IQR, 0.06 to 0.42). Within-tumor correlations between pS6 and stathmin were generally weak (median r, –0.01; IQR –0.17 to 0.18).

The observation that tumors with high heterogeneity tended to get assigned average PI3K scores raised the question whether a subpopulation of cells with high PI3K scores could be masked within the larger tumor bulk that was also additionally comprised of low-PI3K cells. By re-defining each tumor's PI3K score as the median value of the 100 tumor cells with the highest PI3K scores, we made it robust to the potential presence of additional low-PI3K cells. This subset of the cells with the highest PI3K scores per tumor had similarly strong associations with transcriptional signatures and disease progression as the overall score (Fig. S5.D–E; Table S3).

Machine learning

Principal components analysis of the cell-level PTEN, pS6, and stathmin intensities resulted in two factors with comparable eigenvalues (Fig. S6.A). Factor one was positively loaded with all three markers, likely indicating overall immunofluorescence intensity and antigen retrieval success (Fig. 4.C). It was inversely associated with PTEN immunohistochemistry and not associated with transcriptome signatures of PI3K activation (Fig. S6.B–D). Factor two was positively loaded with pS6 and stathmin and negatively loaded with PTEN (Fig. 4.C). This factor was associated with transcriptome signatures of PI3K activation and PTEN immunohistochemistry (Fig. S6.E–G). The close correlation of this factor with mechanistically informed PI3K scores (*r*, 0.85; 95% CI, 0.83 to 0.86; Fig. 4.D) lent the latter additional empirical support.

To further relax the assumptions made thus far, including the linearity assumption made by principal components analysis, we used a big-data implementation of *k* medoids-based clustering to detect distinct cell populations with high PI3K activation (Fig. 4.E; Table S4). A quarter of the tumors were classified, based on the mode of their cell-level cluster value, into a cluster characterized by high PTEN and low pS6 and stathmin expressions (cluster 3). Additional clusters included those with predominantly high pS6 and intermediate-to-high stathmin (cluster 1) and high PTEN and stathmin (cluster 2). A cluster with low PTEN and intermediate pS6 (cluster 5) as well as a cluster with low PTEN and intermediate pS6 and stathmin (cluster 4) most closely resembled our mechanistically informed score.

Comparisons with bulk assessments of transcriptome signatures and PTEN immunohistochemistry provided some support for the validity of clusters 4 and 5 as potential indicators of PI3K activation (Fig. S7.A–B). Consistent with previous results, prognosis of patients with tumors in clusters 4 and 5 was on average worse than in cluster 3 (Table S4). However, there was a high degree of admixture; a median of 43% of cells within each tumor (IQR, 29 to 55%) did not belong to the main cluster the tumor was assigned to.

We tested the robustness of clustering by performing it independently in tumors from the HPFS cohort (*n*, 679) and from the PHS cohort (*n*, 322). There were considerable differences in at least one coordinate for four of the five centroids between these large two sets of tumors (Table S4). Collectively, the exploratory unsupervised analyses supported our subject matter-based PI3K scores and yielded no major additional insight.

References

29. Creighton CJ, Fu X, Hennessy BT, Casa AJ, Zhang Y, Gonzalez-Angulo AM*, et al.* Proteomic and transcriptomic profiling reveals a link between the PI3K pathway and lower estrogen-receptor (ER) levels and activity in ER+ breast cancer. Breast Cancer Res **2010**;12(3):R40 doi 10.1186/bcr2594.

30. Saal LH, Johansson P, Holm K, Gruvberger-Saal SK, She QB, Maurer M*, et al.* Poor prognosis in carcinoma is associated with a gene expression signature of aberrant PTEN tumor suppressor pathway activity. Proc Natl Acad Sci U S A **2007**;104(18):7564-9 doi 10.1073/pnas.0702507104.

45. Rousseeuw PJ, Kaufman L. Finding groups in data. Hoboken: Wiley; 1990.

46. van der Maaten L. Accelerating t-SNE using Tree-Based Algorithms. The Journal of Machine Learning Research **2014**;15(1):3221-45.

Supplementary Tables

Supplementary Table 1. Primary antibodies.

Supplementary Table 2. The prostate cancer PI3K/PTEN signature from The Cancer Genome Atlas primary prostate cancer dataset.

Supplementary Table 3. Sensitivity analyses of different definitions of a PI3K score and lethal prostate cancer.

Supplementary Table 4. Unsupervised clustering of cell-level PI3K markers in the combined prostate cancer cohorts from HPFS and PHS combined (top) and separately in each cohort.

Supplementary Table 1. Individual biomarkers and antibodies.

#	*Antigen*	*Antibody manufacturer*	*Clone*	*Catalog #*	*Dilution*	*Channel*
1	PTEN	Cell Signaling Technology	D4.3	#9188	1:250	CY3
2	Phospho-S6 ribosomal protein Ser 235/236	Cell Signaling Technology	D57.2.2E	#4858	1:500	FITC
3	Stathmin	Cell Signaling Technology	Polyclonal	#3352	1:200	Coumarin
4	Alpha-methylacyl-CoA racemase, P504S	Zeta Corporation	13H4	#D9E	1:250	CY5
5	DAPI	Life Technologies		R37606		Nuclear counterstain

Supplementary Table 2. The prostate cancer PI3K/PTEN signature from The Cancer Genome Atlas primary prostate cancer dataset (n = 333), derived as the top 100 genes from linear models adjusting for *TMPRSS2:ERG* status (binary) and Gleason grade (categorical). The ratio and its 95% confidence interval (CI) denote the "fold change" in gene expression between tumors with *PTEN* copy number alterations (category 1, heterozygous; category 2, homozygous) and/or *PTEN*, *PIK3CA*, and/or *PIK3CB* mutations (all category 2) and tumors without such alterations (category 0), modelled as an ordinal exposure. The last column indicates if the gene is also present in the Creighton PI3K signature.

Gene	*Ratio*	*95% CI*		*-log*$_{10}$ p	*-log*$_{10}$ q *(FDR)*	*Sign*	*Creighton signature*
PTEN	0.58	0.54	to 0.61	50.3	46.6	Downregulated	
PTENP1	0.62	0.58	to 0.66	42.6	39.2	Downregulated	
ATAD1	0.62	0.58	to 0.67	32.8	29.5	Downregulated	
GLUD1	0.78	0.74	to 0.82	18.3	15.1	Downregulated	
GP2	2.44	1.97	to 3.03	14.0	10.9	Upregulated	
FAM35A	0.83	0.79	to 0.87	12.8	9.9	Downregulated	
ANO10	1.13	1.09	to 1.17	11.4	8.5	Upregulated	
MINPP1	0.80	0.75	to 0.85	11.3	8.5	Downregulated	
PIK3R3	1.20	1.14	to 1.27	11.0	8.2	Upregulated	
TTC7B	0.81	0.76	to 0.86	11.0	8.2	Downregulated	
ABHD12	1.26	1.18	to 1.34	10.2	7.5	Upregulated	
ATP11A	1.39	1.26	to 1.53	10.1	7.4	Upregulated	
ENC1	1.28	1.19	to 1.37	10.0	7.3	Upregulated	
TBX3	0.80	0.75	to 0.85	9.9	7.2	Downregulated	
PEX10	1.40	1.27	to 1.55	9.8	7.2	Upregulated	
RSPH1	1.38	1.25	to 1.52	9.7	7.1	Upregulated	
PDIA4	1.19	1.13	to 1.26	9.4	6.9	Upregulated	
C1orf115	0.79	0.73	to 0.85	9.0	6.5	Downregulated	
BECN1	1.09	1.06	to 1.13	8.7	6.2	Upregulated	
TMEM106C	1.18	1.12	to 1.24	8.6	6.2	Upregulated	
MAGED1	1.17	1.12	to 1.24	8.4	6.0	Upregulated	
NOMO1	1.14	1.09	to 1.19	8.4	6.0	Upregulated	
ARF3	1.08	1.05	to 1.10	8.4	6.0	Upregulated	
KPNA2	1.19	1.13	to 1.26	8.4	6.0	Upregulated	
GNPDA1	1.11	1.07	to 1.15	8.3	5.9	Upregulated	
PSMD2	1.09	1.06	to 1.13	8.2	5.8	Upregulated	
EFTUD1	1.12	1.08	to 1.17	8.0	5.7	Upregulated	
HMGB3	1.15	1.10	to 1.21	8.0	5.7	Upregulated	
SLC37A1	1.21	1.14	to 1.30	8.0	5.7	Upregulated	
ANXA5	1.12	1.08	to 1.16	7.9	5.7	Upregulated	
PHYH	1.14	1.09	to 1.20	7.9	5.6	Upregulated	
CD24	1.37	1.23	to 1.52	7.8	5.6	Upregulated	
CD276	1.17	1.11	to 1.24	7.7	5.5	Upregulated	
CCDC6	1.16	1.10	to 1.22	7.7	5.4	Upregulated	
KHDRBS3	1.39	1.24	to 1.55	7.6	5.4	Upregulated	
PGD	1.12	1.08	to 1.16	7.6	5.4	Upregulated	
PSMD6	1.08	1.05	to 1.12	7.5	5.3	Upregulated	
SUB1	1.11	1.07	to 1.16	7.5	5.3	Upregulated	
TSTA3	1.20	1.12	to 1.27	7.5	5.3	Upregulated	
UGDH	1.23	1.14	to 1.32	7.5	5.3	Upregulated	
PRSS8	1.21	1.13	to 1.29	7.5	5.3	Upregulated	
FKBP1A	1.16	1.10	to 1.22	7.4	5.3	Upregulated	
ARF4	1.11	1.07	to 1.15	7.4	5.3	Upregulated	Included
COPB2	1.13	1.08	to 1.18	7.4	5.2	Upregulated	
PCGF5	0.88	0.84	to 0.92	7.4	5.2	Downregulated	

PLA2G2A	1.94	1.53	to 2.44	7.3	5.2	Upregulated	
KLHDC1	0.84	0.79	to 0.89	7.3	5.2	Downregulated	
COPA	1.10	1.06	to 1.14	7.3	5.2	Upregulated	
SEMA3C	0.76	0.69	to 0.83	7.2	5.2	Downregulated	
CTNNA1	1.07	1.04	to 1.09	7.2	5.1	Upregulated	
EEF2K	0.89	0.85	to 0.93	7.2	5.1	Downregulated	
LRRC31	2.04	1.58	to 2.64	7.2	5.1	Upregulated	
PSAP	1.10	1.07	to 1.14	7.2	5.1	Upregulated	
RRM2	1.37	1.22	to 1.53	7.1	5.1	Upregulated	
TFG	1.09	1.05	to 1.12	7.1	5.1	Upregulated	
LAMP1	1.10	1.06	to 1.14	7.0	5.0	Upregulated	
LRRC16A	1.16	1.10	to 1.23	7.0	5.0	Upregulated	
RNF144B	1.22	1.14	to 1.32	6.9	4.9	Upregulated	
IFNGR2	1.10	1.06	to 1.14	6.9	4.9	Upregulated	
PIAS3	1.09	1.06	to 1.13	6.9	4.9	Upregulated	
STX6	1.09	1.05	to 1.12	6.9	4.9	Upregulated	
GAS5	0.81	0.75	to 0.87	6.8	4.8	Downregulated	
ADARB1	0.88	0.84	to 0.92	6.8	4.8	Downregulated	
FAM171A1	1.16	1.10	to 1.23	6.8	4.8	Upregulated	
NT5C2	0.90	0.87	to 0.94	6.7	4.7	Downregulated	
ARRB1	0.87	0.83	to 0.92	6.7	4.7	Downregulated	
BHLHE41	1.31	1.18	to 1.45	6.7	4.7	Upregulated	
CDH1	1.18	1.11	to 1.26	6.6	4.7	Upregulated	
FAM98A	1.08	1.05	to 1.11	6.6	4.7	Upregulated	
LRRC59	1.10	1.06	to 1.14	6.6	4.6	Upregulated	Included
SEC24D	1.16	1.10	to 1.22	6.5	4.6	Upregulated	
CMTM6	1.11	1.07	to 1.16	6.4	4.5	Upregulated	
HEXB	1.18	1.11	to 1.25	6.4	4.5	Upregulated	
HYOU1	1.16	1.10	to 1.23	6.4	4.5	Upregulated	
NOV	1.46	1.26	to 1.68	6.4	4.5	Upregulated	
ZBTB16	0.79	0.72	to 0.86	6.4	4.5	Downregulated	
VCP	1.08	1.05	to 1.12	6.4	4.5	Upregulated	
GANAB	1.09	1.05	to 1.12	6.3	4.4	Upregulated	
CMPK1	1.12	1.07	to 1.17	6.3	4.4	Upregulated	
PCDHB8	1.57	1.32	to 1.86	6.2	4.4	Upregulated	
SNRNP40	1.09	1.06	to 1.13	6.2	4.4	Upregulated	
ZMPSTE24	1.15	1.09	to 1.21	6.2	4.4	Upregulated	
SLC5A1	1.53	1.30	to 1.80	6.2	4.4	Upregulated	
TWF1	1.10	1.06	to 1.14	6.2	4.4	Upregulated	
CPEB3	0.84	0.78	to 0.90	6.1	4.3	Downregulated	
EPCAM	1.17	1.10	to 1.25	6.1	4.3	Upregulated	
RAB18	1.14	1.08	to 1.20	6.1	4.3	Upregulated	
SPATS2L	1.14	1.08	to 1.20	6.1	4.3	Upregulated	
AGT	1.64	1.35	to 1.99	6.1	4.3	Upregulated	
SEC22B	1.10	1.06	to 1.14	6.1	4.3	Upregulated	
RPN2	1.12	1.07	to 1.18	6.1	4.3	Upregulated	
ECE1	1.15	1.09	to 1.22	6.0	4.2	Upregulated	
CCDC141	0.60	0.49	to 0.74	6.0	4.2	Downregulated	
PXDN	1.19	1.11	to 1.27	5.9	4.1	Upregulated	
CALCOCO1	0.92	0.89	to 0.95	5.9	4.1	Downregulated	
COX15	0.92	0.89	to 0.95	5.9	4.1	Downregulated	
MTCH2	1.09	1.06	to 1.13	5.9	4.1	Upregulated	
CHRNA2	0.70	0.60	to 0.80	5.9	4.1	Downregulated	
AGR3	2.19	1.60	to 2.99	5.8	4.1	Upregulated	
SEMA3D	0.61	0.50	to 0.74	5.8	4.0	Downregulated	

Supplementary Table 3. Sensitivity analyses using different definitions of a PI3K score and hazard ratios (with 95% confidence intervals) for lethal prostate cancer. All analyses are unadjusted except as noted for the two-marker score.

Quartile	*1st (lowest)*	*2nd*	*3rd*	*4th (highest)*
Individual markers				
PTEN[1]	1 (ref.)	1.27 (0.59–2.71)	1.93 (0.95–3.93)	3.76 (1.97–7.17)
pS6	1 (ref.)	1.28 (0.75–2.17)	0.45 (0.22–0.95)	0.93 (0.52–1.67)
Stathmin	1 (ref.)	0.94 (0.49–1.80)	1.20 (0.66–2.21)	1.65 (0.92–2.98)
Two-marker score: PTEN+stathmin				
Unadjusted	1 (ref.)	0.93 (0.42–2.04)	1.51 (0.73–3.10)	4.18 (2.26–7.76)
+ age, Gleason, PTEN IHC[2]	1 (ref.)	0.87 (0.36–2.10)	1.62 (0.71–3.68)	2.59 (1.19–5.65)
PI3K score of top 100 cells	1 (ref.)	0.80 (0.38–1.66)	1.82 (0.98–3.39)	2.23 (1.22–4.06)
PI3K score, by spatial clustering				
Getis–Ord $G \leq$ median	1 (ref.)	1.17 (0.48–2.89)	1.07 (0.42–2.71)	1.86 (0.81–4.26)
Getis–Ord $G >$ median	1 (ref.)	0.72 (0.25–2.06)	2.17 (0.91–5.17)	2.23 (0.95–5.21)
PI3K score, by spatial autocorrelation				
Moran $I \leq$ median	1 (ref.)	1.05 (0.38–2.89)	1.42 (0.57–3.55)	2.32 (1.04–5.19)
Moran $I >$ median	1 (ref.)	0.87 (0.34–2.19)	1.69 (0.71–4.02)	1.40 (0.52–3.75)

[1] Quartiles are reversed for PTEN.

[2] PTEN by tumor-level immunohistochemistry. Covariates were coded as in Table 1.

Supplementary Table 4. Unsupervised *k* medoids-based clustering of cell-level PI3K markers in the combined prostate cancer cohorts from HPFS and PHS combined (top) and separately in each cohort (bottom). Centroid positions for each cluster are denoted by PTEN, stathmin, and pS6 coordinates, which were first scaled to a normal distribution. The number of tumors per cluster, assigned based on the most common cluster (mode) among all cells of each tumor, are shown (*n*), as are event counts and unadjusted rates of lethal disease for tumor assigned to each cluster. In the comparison of separate clustering in each cohort, matching clusters are shown on each line; an asterisk indicates centroid coordinates with absolute differences >0.25 between cohorts are marked with an asterisk (*).

HPFS/PHS		Cluster centroid positions			Lethal disease			
Cluster	*n*	PTEN	Stathmin	pS6	Events	Rate[1]	HR[2]	95% CI
1	104	0.32	0.28	2.52	10	6.6	2.55	(1.10– 5.92)
2	146	1.06	0.90	-0.60	9	4.3	1.66	(0.70– 3.94)
3	300	0.65	-0.38	-0.57	12	2.6	1.00	(ref.)
4	191	-0.63	0.66	0.07	31	11.7	4.50	(2.31– 8.76)
5	260	-0.70	-0.96	-0.07	25	6.4	2.50	(1.25– 4.97)

HPFS alone		Cluster centroid positions[3]			*PHS alone*		Cluster centroid positions[3]		
Cluster	*n*	PTEN	Stathmin	pS6	Cluster[4]	*n*	PTEN	Stathmin	pS6
1	82	*0.42	*0.44	2.42	5	31	*0.03	*-0.07	2.52
2	137	1.11	*0.68	-0.44	2	52	0.88	*1.10	-0.58
3	167	0.47	-0.64	-0.48	1	101	0.68	-0.57	-0.42
4	128	-0.40	0.55	-0.19	4	60	*-0.82	0.53	-0.01
5	165	-0.91	-0.65	-0.20	3	78	-0.81	-0.87	-0.21

[1] Rate of lethal disease, per 1000 person-years.

[2] Hazard ratio with 95% confidence interval.

[3] Clusters in PHS were ordered to match clusters from HPFS as close as possible.

Supplementary Figures

Figure S1. The subject matter-informed PI3K score and modified *H* scores. PTEN contributes inversely to the modified *H* score.

Figure S2. mRNA scores.

(A) PTEN copy number and the Saal/Parsons breast cancer-derived PTEN loss mRNA signature (in TCGA-Prostate cancer)
(B) Tumor-level PTEN and the Saal/Parsons breast cancer-derived PTEN loss mRNA signature (in HPFS/PHS).
(C) *PTEN* copy numbers and the prostate cancer PI3K/PTEN transcriptome signature in the derivation cohort TCGA. Dots in colors other than dark blue indicate *PTEN*, *PIK3CA*, or *PIK3CB*-mutated tumors.
(D) Tumor-level PTEN status and the prostate cancer PI3K/PTEN signature in the validation cohorts HPFS and PHS.
(E) PI3K scores and the Saal signature/Parsons PTEN loss mRNA signature.
(F) *PTEN* copy numbers and the Creighton PI3K inhibitor signature derived using Connectivity Map (CMap) in TCGA.
(G) PI3K scores and the Creighton PI3K inhibitor signature derived using Connectivity Map (CMap).
(H) PTEN by immunofluorescence and prostate cancer PI3K/PTEN signature.
(I) pS6 by immunofluorescence and prostate cancer PI3K/PTEN signature.
(J) Stathmin by immunofluorescence and prostate cancer PI3K/PTEN signature.

Figure S3. PI3K scores and Ki-67. Measured as % positive nuclei.

Figure S4. Lethal disease

(A) Restricted mean survival times comparing the first quartile of PI3K scores with the fourth quartile.
(B) pS6, modelled using restricted cubic splines, and hazard ratios for lethal disease. The reference is set to the median value of pS6.
(C) Top panel: Two-marker PI3K scores (PTEN and stathmin, *x* axis), modelled continuously using restricted cubic splines, and hazard ratios for lethal disease (*y* axis). The solid line with gray 95% CI bands is from an unadjusted model; the dotted line with blue 95% CI bands is from a model adjusted for tumor-level PTEN status by immunohistochemistry. The reference value (hazard ratio, 1) is set to the 25th percentile of the two-marker PI3K score, a value of 39. Lower panel: Distribution of PI3K scores, according to tumor-level PTEN status by immunohistochemistry.
(D) PTEN by immunohistochemistry and two-marker PI3K score (PTEN and stathmin).
(E) Two-marker PI3K score (PTEN and stathmin) and the prostate cancer PI3K/PTEN signature.
(F) Two-marker PI3K score (PTEN and stathmin) and Creighton PI3K inhibitor signature derived using Connectivity Map (CMap).

Figure S5. Intratumoral heterogeneity.

(A) Shannon's entropy, based on quartiles across all tumor cells within each tumor core, and heterogeneity in PI3K scores.
(B) PTEN by immunohistochemistry and heterogeneity in PI3K scores.
(C) Tumor cell count and heterogeneity in PI3K scores.

(D) PTEN by immunohistochemistry and PI3K score defined as the median score of the top 100 cells (with the highest PI3K scores).
(E) PI3K score defined as the median score of the top 100 cells and the prostate cancer PI3K/PTEN mRNA signature.
(F) PI3K scores and spatial clustering of PI3K scores quantified by Getis-Ord *G*.
(G) Tumor cell count and spatial clustering of PI3K scores quantified by Getis-Ord *G*.
(H) PI3K scores and spatial autocorrelation of PI3K scores quantified by Moran's *I*.
(I) PTEN by immunohistochemistry and spatial autocorrelation of PI3K scores quantified by Moran's *I*.
(J) PTEN by immunohistochemistry and spatial autocorrelation of cell-level PTEN immunofluorescence intensity quantified by Moran's *I*.

Figure S6. Machine learning 1: Principal components analysis.

(A) Eigenvalues from principal components analysis
(B) PTEN by immunohistochemistry and the first principal component.
(C) The first principal component and the prostate cancer PI3K/PTEN mRNA signature.
(D) The first principal component and the Creighton PI3K inhibitor signature derived using Connectivity Map (CMap).
(E) PTEN by immunohistochemistry and the second principal component.
(F) The second principal component and the prostate cancer PI3K/PTEN mRNA signature.
(G) The second principal component and the Creighton PI3K inhibitor signature derived using Connectivity Map (CMap).

Figure S7. Machine learning 2: *k*-medoids clustering using CLARA.

(A) CLARA clusters and the prostate cancer PI3K/PTEN mRNA signature.
(B) CLARA clusters and the Creighton PI3K inhibitor signature derived using Connectivity Map (CMap).

Supplementary Figure 1

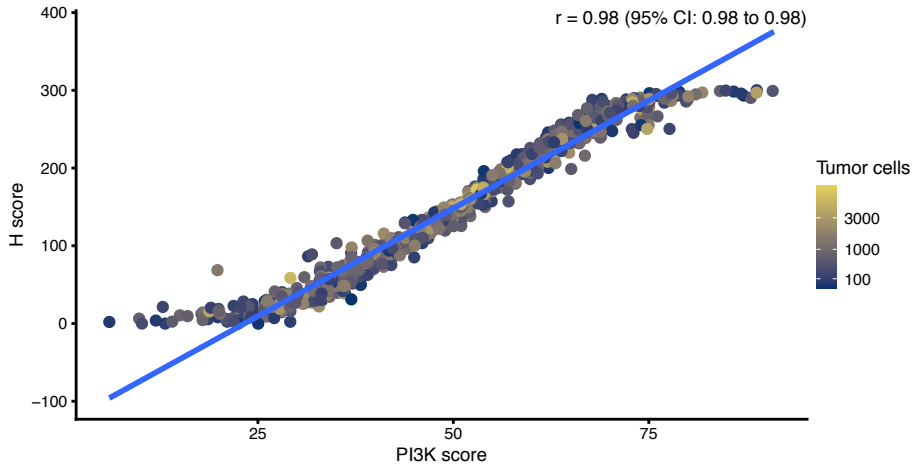

Supplementary Figure 2

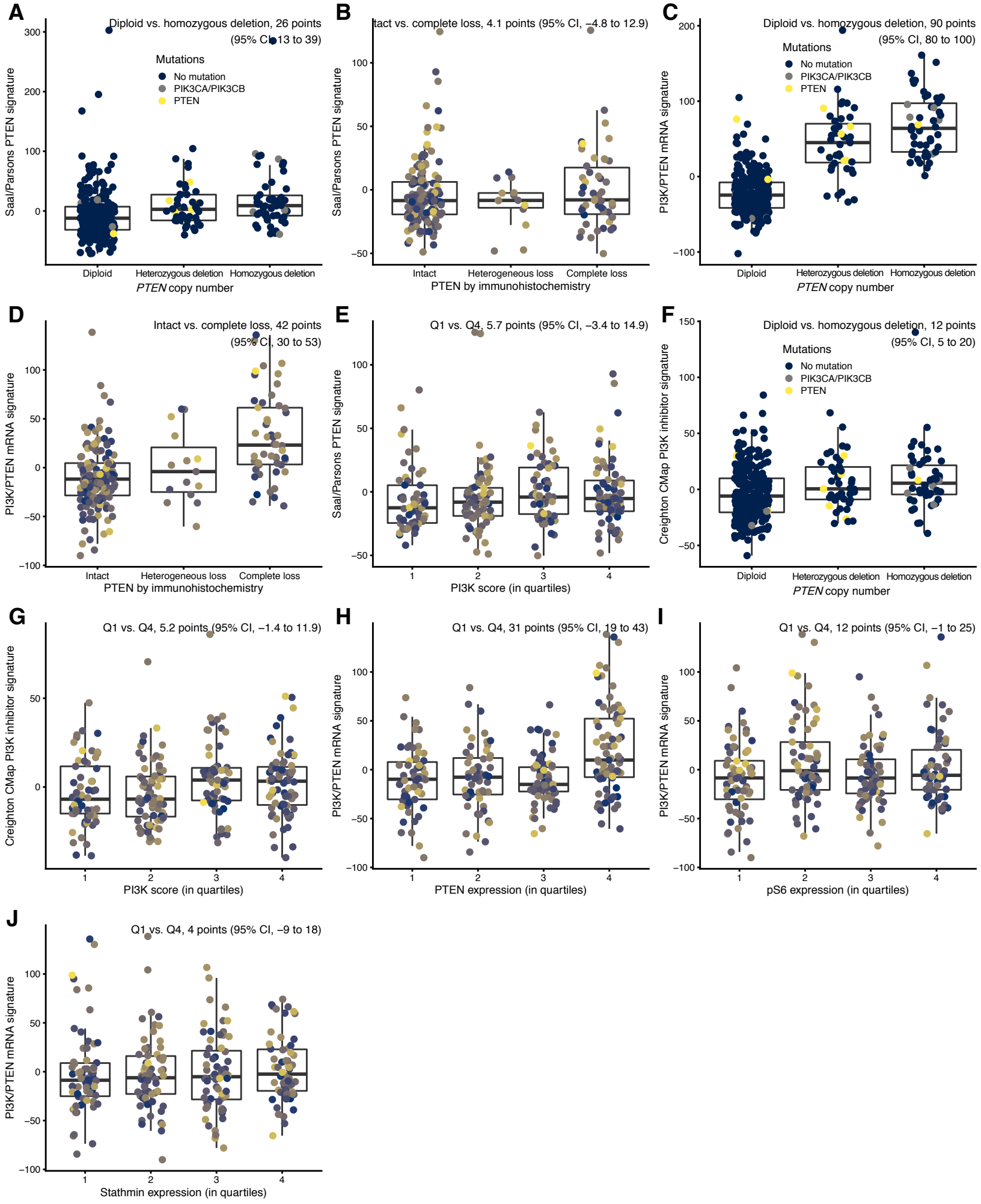

Supplementary Figure 3

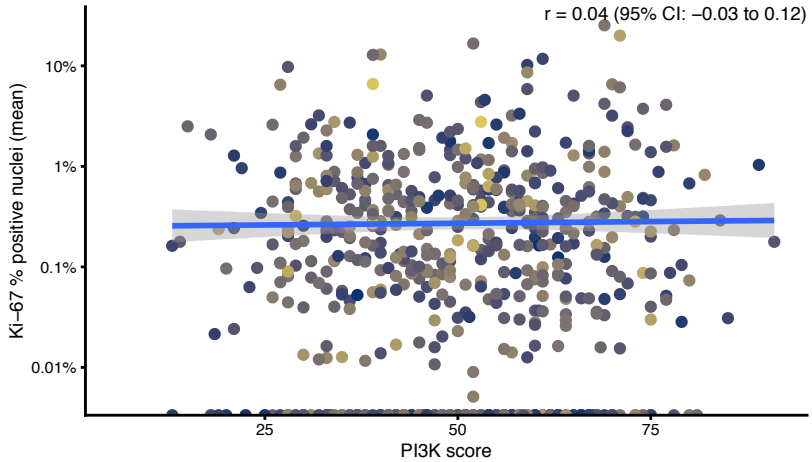

Supplementary Figure 4

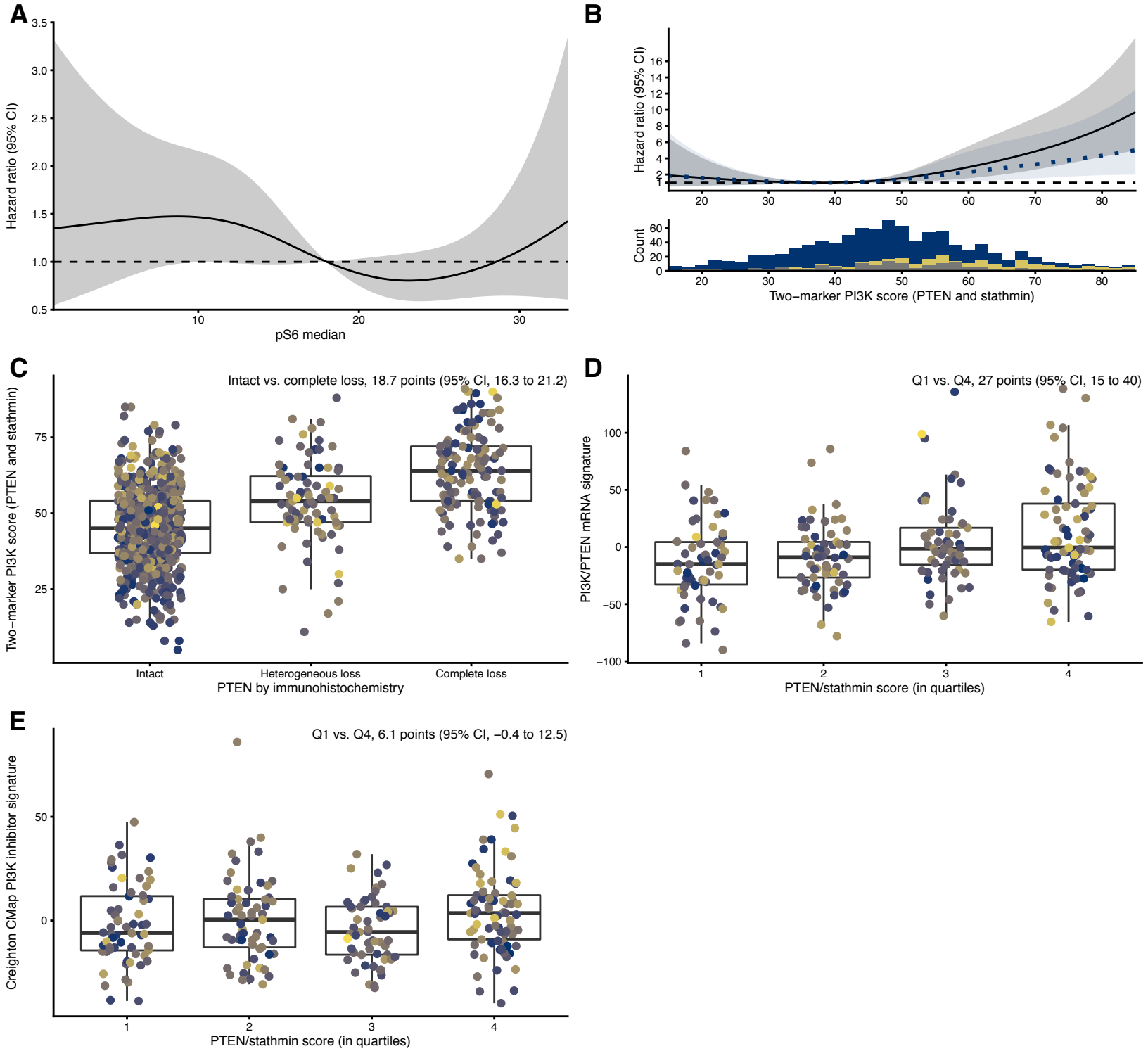

Supplementary Figure 5

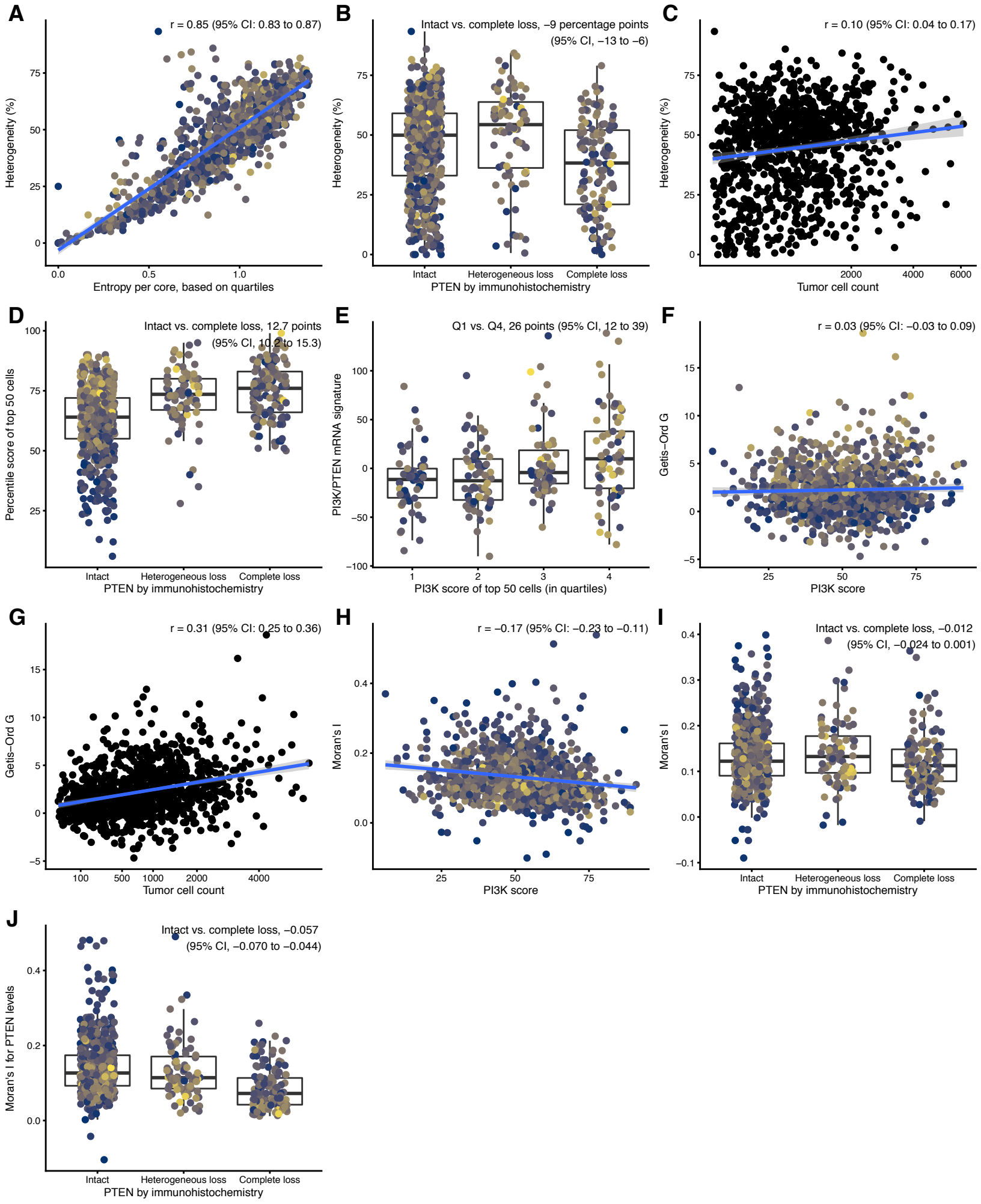

Supplementary Figure 6

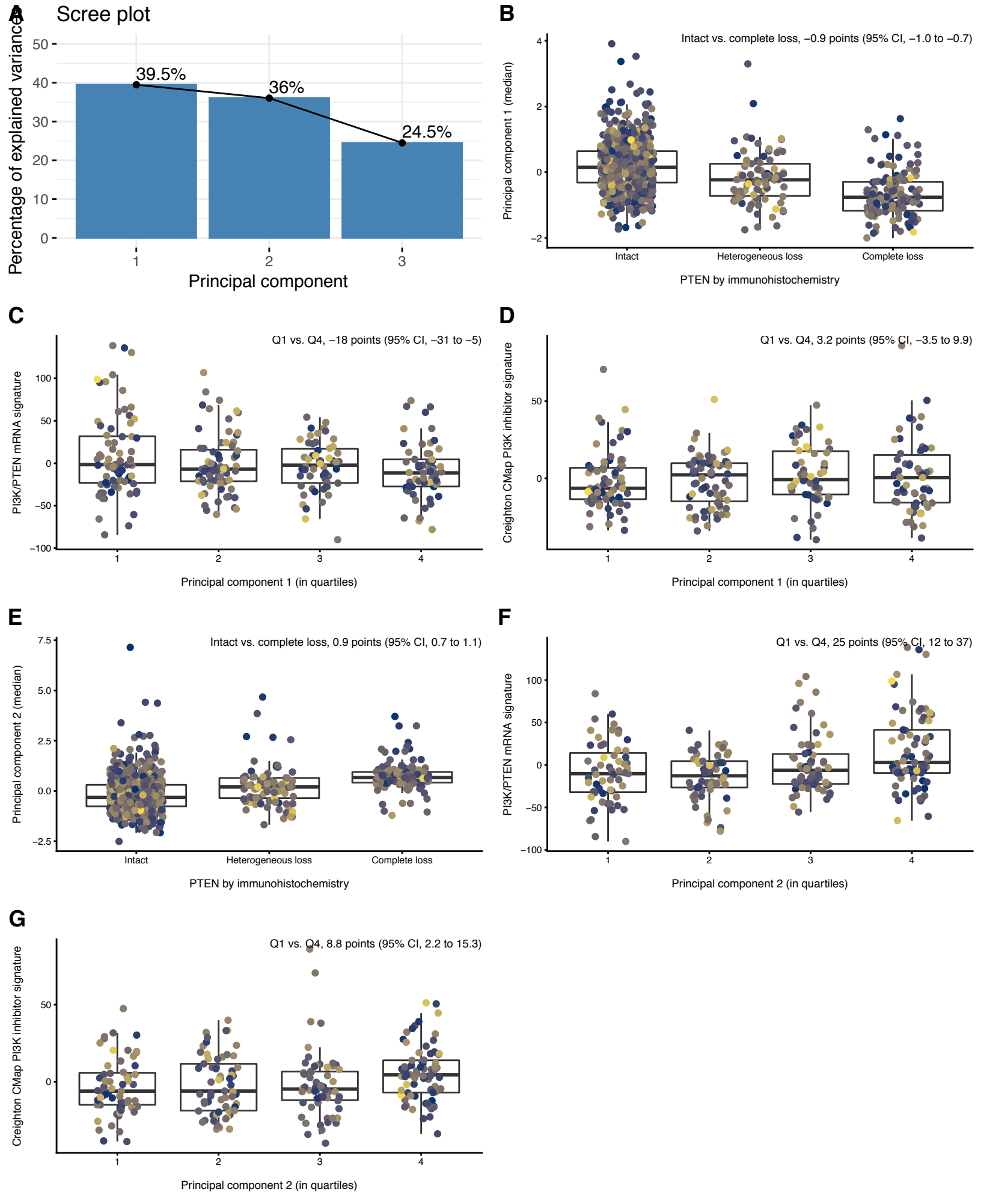

Supplementary Figure 7